Ultrahigh Resolution Structures of Nitrophorin 4: Heme Distortion in Ferrous CO and NO Complexes[†,‡]

Estelle M. Maes, Sue A. Roberts, Andrzej Weichsel, and William R. Montfort*

Department of Biochemistry and Molecular Biophysics, University of Arizona, Tucson, Arizona 85721

Received April 10, 2005; Revised Manuscript Received June 10, 2005

ABSTRACT: Nitrophorin 4 (NP4), a nitric oxide (NO)-transport protein from the blood-sucking insect *Rhodnius prolixus*, uses a ferric (Fe^{3+}) heme to deliver NO to its victims. NO binding to NP4 induces a large conformational change and complete desolvation of the distal pocket. The heme is markedly nonplanar, displaying a ruffling distortion postulated to contribute to stabilization of the ferric iron. Here, we report the ferrous (Fe^{2+}) complexes of NP4 with NO, CO, and H_2O formed after chemical reduction of the protein and the characterization of these complexes by absorption spectroscopy, flash photolysis, and ultrahigh-resolution crystallography (resolutions vary from 0.9 to 1.08 Å). The absorption spectra, both in solution and in the crystal, are typical for six-coordinated ferrous complexes. Closure and desolvation of the distal pocket occurs upon binding CO or NO to the iron regardless of the heme oxidation state, confirming that the conformational change is driven by distal ligand polarity. The degree of heme ruffling is coupled to the nature of the ligand and the iron oxidation state in the following order: (Fe^{3+})-NO > (Fe^{2+})-NO > (Fe^{2+})-CO > (Fe^{3+})-H_2O > (Fe^{2+})-H_2O. The ferrous coordination geometry is as expected, except for the proximal histidine bond, which is shorter than typically found in model compounds. These data are consistent with heme ruffling and coordination geometry serving to stabilize the ferric state of the nitrophorins, a requirement for their physiological function. Possible roles for heme distortion and NO bending in heme protein function are discussed.

Thousands of heme-containing proteins exist in nature, each with a specific function made possible by the specific tuning of the heme moiety. Generally, in such proteins, the heme is partially or fully buried in the protein interior and ligated to the protein through a proximal cysteine, methionine, or histidine. In some cases, the heme is also covalently linked to the protein through the vinyl groups. The protein environment may influence the heme chemical properties in multiple ways, including the restricting of access to the distal (sixth) ligation site, influencing the strength of the proximal ligand bond, altering the electrostatic surface near the heme, and distorting the heme geometry away from planar. In response to these forces, the properties of the heme are altered such that a specific chemical process can be achieved. Without this tuning of the heme by the protein, most heme proteins would fail to carry out their function. Despite the considerable data available on heme proteins, the means by which they achieve their considerable functional diversity remains largely unknown.

One heme property of importance is the reduction potential of the iron center. Oxygen carrier proteins such as myoglobin and hemoglobin require a ferrous (Fe^{2+})[1] heme center for oxygen binding and have evolved to resist oxidation to the ferric (Fe^{3+}) state. Nitric oxide carrier proteins such as the nitrophorins require a ferric heme center to achieve a reversible NO complex and have evolved to resist reduction to the ferrous state. The cytochromes are redox active and cycle between ferric and ferrous states while functioning. Factors that have been proposed as important for setting the heme reduction potential include the electrostatic environment, the properties of the proximal ligand, and distortion of the porphyrin ring.

Nitrophorins from the saliva of the blood-sucking insect *Rhodnius prolixus* (rNP) use a ferric heme to transport NO from the salivary gland of the insect (pH ∼ 5) to the tissue of a victim (pH ∼ 7), where the NO molecule is released in response to higher pH and dilution (*1*). The release of NO in the vicinity of the bite takes advantage of host signaling pathways that lead to vasodilation and reduced platelet aggregation. This, in combination with a host of other antihemostatic salivary proteins released by the insect, facilitates blood feeding by the insect (*2*−*5*). Maintenance of the ferric state is necessary for NO release since the ferrous state has such high affinity for NO ($K_d = 10^{-12}-10^{-15}$) that release is extremely slow, whereas the ferric state has an affinity for NO that allows faster release of the molecule ($K_d = 10^{-6}-10^{-9}$) (*6*).

[†] This work was supported in part by grants from the American Heart Association (E.M.M.) and from the National Institutes of Health (HL62969 to W.R.M.).

[‡] Coordinates for all structures reported have been deposited in the Protein Data Bank (PDB entries 1YWA, 1YWB, 1YWC, 1YWD).

* To whom correspondence should be addressed: William R. Montfort, Department of Biochemistry and Molecular Biophysics, University of Arizona, 1041 E. Lowell St., Tucson, AZ 85721. Telephone: (520) 621-1884. Fax: (520) 621-1697. E-mail: montfort@email.arizona.edu.

[1] Abbreviations: NO, nitric oxide; CO, carbon monoxide; Fe^{3+}, ferric iron; Fe^{2+}, ferrous iron; rNP, *Rhodnius* nitrophorins; NP1−4, *Rhodnius* nitrophorins 1−4.

10.1021/bi0506573 CCC: $30.25 © 2005 American Chemical Society
Published on Web 08/27/2005

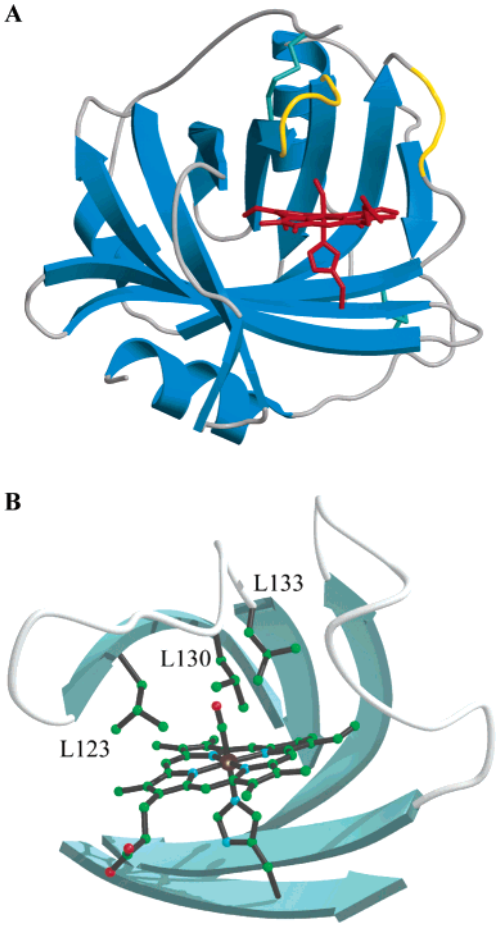

FIGURE 1: Ribbon drawings of NP4. (A) His 59, heme and NO are shown in red. The NO-induced conformational change involves two mobile loops A−B (residues 30−37) and G−H (residues 125−131), shown in gold. (B) Close-up of the heme pocket, showing residues in contact with CO (one heme propionate is deleted for clarity).

Four *Rhodnius* nitrophorins have been characterized and three (NP1, NP2, and NP4) have had their crystal structures determined (*7*−*9*). The rNPs display a lipocalin fold with heme inserted into one end of the lipocalin beta-barrel (Figure 1). At the low pH of the insect salivary gland, NO binding leads to a large conformational change involving loops A−B and G−H, which collapse into the distal pocket and pack hydrophobic side chains against the NO moiety, protecting it from solvent-mediated reduction (*10*). This transition requires a nonpolar ligand such as NO; charged ligands such as CN^- do not induce the closed conformer. At higher pH, such as that of the victim's blood, these loops move out of the distal pocket, facilitating NO release (*6*, *11*, *12*). The rNP structures also display highly distorted heme conformations, with pyrrole rings rotated out of the heme plane.

The reduction potential for heme in unliganded rNP is about −300 mV (*6*), the equivalent of a ferriheme stabilization energy of ∼7 kcal mol^{-1} with respect to the histidine ligated heme in myoglobin. A correlation between heme distortion and reduction potential has been noted for both model compounds and proteins, leading to the suggestion that heme distortion disfavors heme reduction (*4*, *13*−*16*). Crystals of NP4 diffract extremely well, allowing atomic resolution structures to be determined and heme geometry to be refined without model bias (*11*, *12*, *17*). These studies make clear that the NP4 heme adopts a ruffled conformation that becomes more pronounced upon NO ligation and that the NO ligand is bent away from the expected linear state by ∼20°.

Here, we report ultrahigh-resolution crystal structures of ferrous NP4, prepared through chemical reduction, in complexes with water, NO, and CO (which binds only to ferrous heme). We also report the UV−visible spectra for these complexes in both solution and crystal and the kinetics of CO binding. The heme remains distorted in the ferrous complexes, but less so than in the ferric state. Both NO and CO binding increase the heme distortion, suggesting an as yet unexplained electronic role for heme distortion in the nitrophorins.

MATERIALS AND METHODS

Preparation of Protein Samples and Absorption Spectroscopy. NP4 was overexpressed from an *Escherichia coli* strain and refolded from inclusion bodies supplemented with heme, as described previously (*9*, *18*). Chemical reduction of NP4 was achieved by anaerobic addition of freshly prepared sodium dithionite (10-fold excess) after the protein sample in either sodium acetate, pH 5.0, or Tris-HCl, pH 8.0, had been purged with argon. The ferrous CO and NO complexes were prepared by two different methods depending on the final concentration of gas in solution. When low final concentrations of gas were required (25−100 μM), small aliquots of gas-saturated buffer (concentrations of 1.25 and 1.9 mM for CO and NO, respectively) were added to a sealed anaerobic cuvette containing the reduced protein, using a gastight syringe. When higher final concentrations of ligand were required, an appropriate small volume of concentrated reduced protein was added to a CO- or NO-saturated solution.

UV−visible absorption spectra of the protein solutions were recorded under anaerobic conditions at room temperature using a Varian Cary-300 spectrophotometer. Molar extinction coefficients were calculated using the pyridine hemochromogen assay (*19*). A few microliters of protein solution and crystals of dithionite were added to 1 mL of a pyridine (30%)−NaOH (0.1 N) solution. The peak absorbance at 556 nm minus that at 700 nm was used to determine the hemin concentration, assuming an extinction coefficient of 32 mM^{-1} cm^{-1} (*19*) and a protein/heme molar ratio of 1.

The visible absorption spectra of protein crystals, the preparation of which is described below, were obtained under anaerobic conditions in sealed capillaries at room temperature. Measurements were carried out at room temperature using a microspectrophotometer assembled in-house, consisting of an optical stage with focusing optics (4DXray Systems), a xenon lamp, and a CCD-based spectrophotometer (Spectral Instruments). Light from the lamp was focused into a quartz fiber optic cable connected to the optical bench. The source entered a reflective objective (to retain UV light) and was focused to ∼25 μm at the sample, which was typically not more than 0.1 mm thick. The transmitted light was gathered by a second objective and led into the CCD detector with a second quartz fiber.

Kinetics. All measurements were performed in solution at room temperature under pseudo-first-order conditions. Photolysis of CO (in solutions with CO concentrations of 25 μM to 1.25 mM, pH 8.0) was initiated at 396 nm by a pulsed Photochemical Research Associates nitrogen dye laser

(500 ps and 0.1 mJ/pulse) using POPOP (0.39 g/mL) in toluene as the dye. The progress of the reaction was monitored at 440 nm and recorded with a Tektronix TDS 410A oscilloscope, averaging 7−13 separate transients. The observed rate constant for CO rebinding (k_{obs}) was calculated with a single-exponential fit to the experimental data using the software KinFit (Olis, Inc., Bogart, GA), and then taking the average of three measurements at each of three CO concentrations. The second-order rate constant k_{on} was obtained through fitting of the average k_{obs} values to eq 1 using SigmaPlot (SPSS, Inc., Chicago):

$$k_{obs} = k_{on}[CO] + k_{off} \quad (1)$$

Crystallization and Diffraction Data Measurement. NP4 crystals were grown at room temperature in 2.8 M ammonium phosphate, pH 5.6 or 7.5, using the hanging drop method, as described previously (*10*, *17*). To obtain crystals in the ferrous state, protein crystals were first soaked in an argon-saturated potassium phosphate solution (3.2 M, pH 7.1) and then reduced with an anaerobic solution containing sodium dithionite (20 mM) and potassium phosphate (3.2 M). To produce the ferrous CO or NO complex, NP4 (Fe^{2+}) crystals were transferred to a septum-sealed test tube containing a potassium phosphate solution (3.2 M, pH 5.6 or 7.1) that had been saturated with CO or NO, respectively, and soaked for 15 min after supplementing with the appropriate gas. Crystals were either retrieved with a cryoloop (Hampton) and flash-frozen in liquid nitrogen for X-ray data collection at 100 K or sealed in a capillary under a gaseous atmosphere (CO or NO) for absorption spectroscopy at room temperature. All crystals belonged to the *C*2 space group with cell constants typical of those found for NP4 (Fe^{3+}) complexes, $a = 70.2$ Å, $b = 42.7$ Å, $c = 52.9$ Å, $\beta = 94.2°$ (*17*).

Diffraction data were collected at 100 K on beam line 9-1 of SSRL (Stanford Synchrotron Radiation Laboratory, Palo Alto, CA) using a Mar 345 imaging plate (NP4−H_2O), or on beam line 14 BM-C of the Advanced Photon Source (Argonne National Laboratory, Argonne, IL) with a Quantum-4 CCD detector (NP4−NO and NP4−CO). All data were reduced with Crystal Clear (d*TREK) (*20*).

Structure Determinations. The refined structures of the ferric protein and its complexes with NH_3 or NO (PDB entries 1D2U and 1KOI, respectively) were used as starting models (*17*). Refinement was first performed using REFMAC from the CCP4 package (*21*) and subsequently using SHELX (*22*). Model building was accomplished with the program O (*23*). For the final models, anisotropic *B*-factors were refined and hydrogen atoms included at calculated positions but not refined, resulting in *R*-factors ranging from 0.12 to 0.14. For certain residues, alternative positions were indicated in electron density maps and added to the models. All main-chain atoms of the alternate conformer were added to preserve stereochemistry. The occupancy of protein conformers was refined, while that of disordered solvent was fixed at 0.5, except for those linked to protein conformers.

To model the heme without planar restraints and obtain an estimate of the standard deviations in the heme coordination geometry, full-matrix least squares refinement was applied to the final models using SHELX (*22*), with the proximal histidine (His 59), the axial ligand (H_2O, CO, or NO), and the iron coordination sphere refined without restraint but all other atoms fixed. This method also allowed us to calculate the heme atom deviations from the least squares heme plane, with associated errors.

To further quantify the degree of heme distortion in each structure, the normal coordinate structural decomposition (NSD) method developed by Shelnutt and co-workers was applied (*24*). Using the NSD method, we report the mean out-of-plane displacement of the heme atoms, in angstroms, along the normal modes for ruffling (corresponding to the out-of-plane vibrational mode of B_{1u} symmetry) and saddling (B_{2u}). MOLSCRIPT (*25*), BOBSCRIPT (*26*), and RASTER3D (*27*) were used to prepare figures.

Table 1: UV−Visible Absorption Maxima (nm) and Extinction Coefficients (mM^{-1} cm^{-1}) for NP4 and Horse Heart Myoglobin at pH 8.0

complex	Soret	α	β
	NP4		
ferric aqua[a]	404 (141.4 ± 2.6)[b,c]	np[d]	np[d]
ferrous aqua	426 (102)	np[d]	557 (14)
ferric NO	420 (121)	568 (12)	532 (11)
ferrous NO	416 (93)[e]	571 (10)[e]	547 (10)[e]
ferrous CO	420 (144)[e]	564 (7)[e]	540 (8)[e]
	Mb[f]		
ferric aqua[g]	408 (188)	np[d]	np[d]
ferrous aqua	435 (121)	np[d]	560 (13.8)
ferric NO	420.5 (155)	572 (10.3)	530 (10.5)
ferrous NO	421.5 (147)	575 (10.5)	543 (11.6)
ferrous CO	424 (207)	579 (13.9)	540 (15.4)

[a] Additional bands at 627 and 498 nm. [b] Unless otherwise noted, the extinction coefficient in parentheses was determined using the pyridine hemochrome method (see Materials and Methods). [c] The error was obtained from four replicated sets of experiments. [d] Not present or indistinct. [e] The extinction coefficient was calculated by using an $\epsilon = 141$ mM^{-1} cm^{-1} for the Soret peak of NP4 (Fe^{3+}). [f] Taken from ref *19*. [g] Additional bands at 630 and 502 nm.

RESULTS

We have examined the structure, kinetic and spectroscopic features of ferrous NP4 in complexes with H_2O, NO, and CO to aid in understanding how the ferric state is stabilized and the binding of hydrophobic ligands induces the closed protein conformation.

UV−Visible Absorption Spectroscopy of NP4 Solutions and Crystals. The solution absorption spectra of the aqua and nitrosyl adducts of ferric and ferrous rNPs have been previously reported (*6*, *18*), the ferrous spectra having been obtained after electrochemical reduction (*6*, *28*). Here, we report the optical spectra of ferrous NP4 complexed with H_2O, NO, and CO in both solution and crystalline states after reducing the ferric protein with sodium dithionite. Molar extinction coefficients of these complexes were measured in solution using the pyridine hemochrome method (see Materials and Methods).

The absorption maxima and extinction coefficients for NP4 and myoglobin (Mb) complexes, pH 8.0, are listed in Table 1, and the solution absorption spectra for NP4 are shown in Figure 2A. As previously described (*6*, *9*), NP4 (Fe^{3+})−H_2O exhibits spectral features that are found in other histidine-coordinated heme proteins, notably an intense, sharp Soret band at ~400 nm, broad α- and β-bands at ~550 nm, and a weaker band at ~630 nm. When NO binds, the Soret band

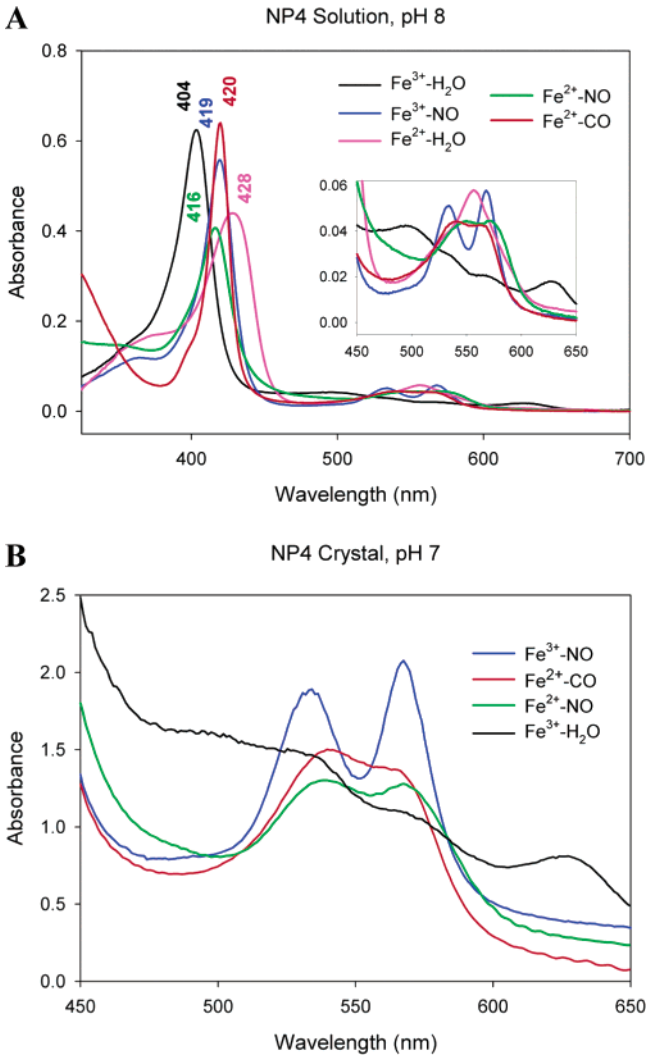

FIGURE 2: Solution and crystal UV−visible absorption spectra. (A) Solution spectra of NP4 recorded at room temperature (pH 8.0). Shown are (Fe^{3+})−aqua (black) and NP4 (Fe^{3+})−NO (green), and after reduction with 10-fold excess sodium dithionite, (Fe^{2+})−aqua (pink), (Fe^{2+})−CO (60 μM, red), and NO (100 μM, blue), with Soret maxima indicated. Inset: expanded view of Q-band region. (B) Crystal spectra of NP4 (Q-band).

red-shifts to near 420 nm, the intensities of the α- and β-bands increase, and that of the 630 nm-band recedes, a behavior typical of ferric nitrosyl heme proteins.

Reduction of the NP4 heme through the anaerobic addition of a 10-fold excess of sodium dithionite is accompanied by a broadening and red-shift of the Soret peak to near 428 nm (Figure 2A), similar to that observed by applying a negative potential to the ferric form (*6*). As previously noted (*6*), this species is unstable and the Soret absorbance maximum blue-shifts by several nm within a few minutes, most likely reverting to the ferric state. In contrast, the 26 nm red-shift of the metmyoglobin Soret after reduction with dithionite is quite stable ((*19*, *29*), E. M. Maes and W. R. Montfort, unpublished observations).

The binding of CO to reduced NP4 in solution causes the Soret band to blue-shift, sharpen, and increase in intensity, indicating formation of a six-coordinate, low-spin heme. Changes in the spectrum when CO binds are also apparent in the α- and β-band region (Figure 2A, Table 1). Likewise, binding of NO to reduced NP4 elicits absorption maxima that are consistent with a six-coordinate, low-spin ferrous complex (Figure 2A, Table 1) (*19*, *29*). Overall, the spectral characteristics observed for the CO and NO complexes of ferrous NP4 are qualitatively similar to those of ferrous myoglobin, hemoglobin, and a variety of other histidine-ligated heme proteins (*19*, *29*, *30*), with the exception of the α-band of NP4−CO being blue-shifted relative to that of Mb−CO (Table 1), and the difference in the Soret band positions of the ferric and ferrous NO complexes, which is larger for NP4 than for Mb (Table 1), a behavior also noted for NP1 (*6*, *28*).

The extinction coefficients at the Soret for NP4 are smaller by 10−20% than those reported in the literature for sperm whale myoglobin (*19*, *29*) and 15−35% smaller than those reported for horse heart myoglobin (Table 1; (*19*)), but otherwise similar to the globins. Upon binding CO to ferrous NP4, there is a sharp increase in the extinction coefficient, but as with the globins, NO binding leads to little change in extinction coefficient magnitude. The difference in extinction coefficient values between the Fe^{3+}−NO and Fe^{2+}−NO complexes is larger for NP4 (Table 1) and NP1 (*28*) than for Mb, while the difference between the Fe^{2+}−H_2O and Fe^{2+}−CO species is smaller.

Armed with the solution absorption behavior, we could now clearly monitor complex formation in the crystal using a microspectrophotometer (Figure 2B). Because the crystals are optically dense, the Soret band is generally too intense to be measured, and the Q-band region must be used for characterization. Conditions were identified that yielded NP4 complexes with essentially identical absorption spectra in the crystalline state (Figure 2B) to those in solution (Figure 2A), giving confidence that the desired complex was indeed formed in the crystal. The crystal spectroscopy proved especially useful for finding conditions to generate the correct heme oxidation state in the crystal and for fully saturating ligand binding, which occurs more slowly in the crystal than in solution.

Kinetics of CO Binding. NO binding to ferric NP is multiphasic under all conditions, even after mutation to active-site loops A−B and G−H, which undergo large changes in conformation during binding (*6*, *11*, *31*). To address whether CO binding is also multiphasic, we examined CO binding rates using flash photolysis. The initial, concentration-dependent CO binding to ferrous NP4 at pH 8.0 was found to be 7.9 ± 1.4 μM^{-1} s^{-1}, a value 10-fold larger than that reported for sperm whale myoglobin (0.5 μM^{-1} s^{-1}) (*32*) and 3-fold larger than for NO binding to ferric NP4 (~2.5 μM^{-1} s^{-1} at pH 8.0 (*6*, *11*)). As with NO binding to ferric NP4, a second kinetic phase was apparent for CO binding but could not be accurately assessed by flash photolysis. Attempts to measure both phases by stopped-flow spectroscopy were unsuccessful due to the instability of ferrous NP4.

Structure of Ferrous NP4−H_2O at pH 7.1. A crystal of NP4 grown in 2.8 M ammonium phosphate solution was soaked in 3.2 M potassium phosphate and reduced with dithionite to produce the ferrous aqua complex. A color change occurred during the potassium phosphate soak, indicating the replacement of ammonia at the distal ligation site with water. We determined the structure of NP4 (Fe^{2+})−H_2O to 1.08 Å resolution at pH 7.1 (Table 2, Figure 3A) and compared it to that of NP4 (Fe^{3+})−NH_3 at pH 7.5 (*17*).

Table 2: X-ray Data Measurement and Refinement Statistics for Ferrous NP4 Complexes

ferrous complex	H_2O	CO		NO
PDB ID	1YWD	1YWA	1YWC	1YWB
pH	7.1	5.6	7.4	5.6
wavelength (Å)	0.75	0.9	0.9	0.9
resolution (Å)	30−1.08	19−0.89	22−1.0	28−0.97
total no. of reflections	331856	348741	228686	217232
no. of unique reflections	65725	107559	77142	87670
completeness (%)[a]	99/98	90/70	92/76	96/93
mean I/σ_I[a]	9.1/2.0	26.9/3.6	29.0/10.9	7.6/2.7
R_{sym}[a,b]	0.052/0.23	0.038/0.20	0.040/0.13	0.052/0.46
rmsd bonds (Å)	0.014	0.015	0.015	0.015
rmsd angles (Å)	0.035	0.034	0.033	0.033
no. of multiple conformers	9	19	19	13
R_{cryst}/R_{free}[c]	0.14/0.17	0.12/0.15	0.12/0.15	0.14/0.17

[a] Overall/outermost shell. [b] $R_{sym} = (\sum_h|I_h - \langle I\rangle|)/(\sum_h I_h)$, where $\langle I\rangle$ is the mean intensity of all symmetry-related reflections I_h. [c] $R_{cryst} = (\sum|F_{obs} - F_{calc}|)/\sum F_{obs}$. R_{free} as for R_{cryst}, using a random subset of the data (5%) not included in the refinement.

The high resolution of the data allowed us to obtain unrestrained refinement of the iron coordination geometry (Table 3) and accurate assessment of heme distortion (Table 4). Overall, the two structures are very similar in that the distal heme cavity is open with residues 31−37 (loop A−B) poorly ordered and residues 125−133 (loop G−H) located away from the heme pocket. The largest difference between the structures is a lengthening of the iron−H_2O bond in the ferrous structure (2.20 (3) Å, Table 3) compared to the iron−NH_3 bond in the ferric structure (2.06 (2) Å). The temperature factor of the H_2O ligand is high relative to the surrounding atoms, implying that the ligation site is only partially occupied. Close examination of the heme coordination geometry revealed additional structural differences at the iron center. While the metal lies roughly in the porphyrin plane in the oxidized state, it moves out of the plane toward the proximal histidine by 0.1 Å in the reduced state. Both the lengthening of the bond between ferrous iron and the weaker axial ligand and the movement of the iron atom out of the heme plane toward the stronger ligand are typical of ferrous complexes.

In contrast to most six-coordinate porphyrin systems, for which the macrocycle is generally planar in the absence of bulky peripheral substituents (*13*), rNPs have ruffled hemes (*17*), which may serve to stabilize the ferric state. In the present structure, the Fe^{2+} heme of NP4 is still markedly nonplanar, but less so than in the ferric state. We used the normal-coordinate structural decomposition (NSD) approach of Shelnutt and co-workers (*13*) to quantify the heme distortion (Table 4). In the (Fe^{2+})−H_2O complex, the heme is both ruffled and saddled, with the same magnitude for both distortions, but the ruffling distortion is smaller than that observed in the equivalent ferric complex.

Structure of NP4−CO at pH 5.6. Obtaining fully saturated NP4 (Fe^{2+})−CO crystals required developing specific handling conditions. Initial attempts were not satisfactory as judged by the electron density of the axial ligand in X-ray structures and the absorption spectra. This is most likely due to the instability of the ferrous state and the volatility of CO. Success was achieved by minimizing the contact of the reduced crystal with air during its transfer into the CO-saturated solution, by supplementing the tube to which the crystal was transferred with CO gas and by monitoring complex saturation with the microspectrophotometer.

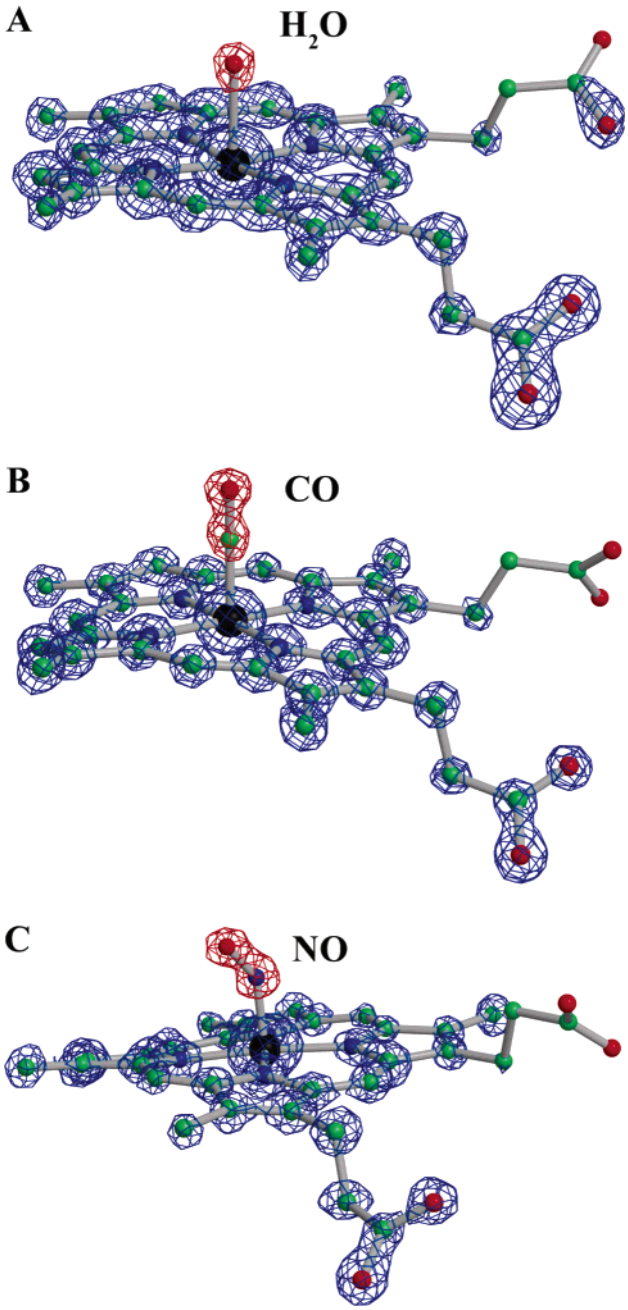

FIGURE 3: Electron density ($2F_o - F_c$) for heme (blue) and distal ligands (red). (A) Ferrous aqua complex. (B) Ferrous CO complex (pH 5.6). (C) Ferrous NO complex. While the ligands and heme core adopt a single conformation, one heme propionate is less well-ordered.

We determined the crystal structures of NP4−CO at pH values of 5.6 (this section) and 7.4 (next section) to resolutions of 0.89 and 1.0 Å, respectively. The most significant difference between the ferrous aqua and the CO complexes is the heme pocket conformation, which is closed and desolvated in the presence of CO, particularly at pH 5.6. The binding of CO to Fe^{2+} heme at pH 5.6 causes loops G−H and A−B to move near the heme and the carbonyl peptide group of Leu 130 to form a hydrogen bond with the carboxylate group of Asp 30, just as is observed when NO

Table 3: Ferrous Iron−Ligand Bond Distances and Angles[a]

	ferrous complex			
atoms	H_2O, pH 7.1	CO, pH 5.6	CO, pH 7.4	NO, pH 5.6
Fe−ligand	2.20 (3)	1.814 (9)	1.79 (1)[b]	1.73 (1)
Fe−Nϵ2	2.01 (1)	2.002 (6)	1.986 (8)	2.11 (1)
Fe−NA	2.01 (1)	1.975 (8)	1.98 (1)	1.99 (1)
Fe−NB	1.97 (1)	1.987 (7)	1.96 (1)	2.00 (1)
Fe−NC	2.00 (2)	2.004 (7)	1.99 (1)	2.00 (1)
Fe−ND	1.99 (2)	1.968 (8)	1.98 (1)	2.03 (1)
X−O	n/a[c]	1.11 (1)	1.12 (2)	1.15 (1)
Fe-X−O	n/a[c]	177 (1)	173 (2)	141 (1)

[a] Numbers in parentheses are estimated errors obtained from full-matrix (block-diagonal) inversion after unrestrained refinement of the proximal histidine, heme, and the axial ligand (*22*) (see Materials and Methods). [b] This structure was refined with a CO occupancy of 0.75 and a H_2O occupancy of 0.25. The Fe−CO geometry was allowed to vary, while the Fe−H_2O bond distance was fixed at 2.1 Å. [c] n/a, not available.

Table 4: Representative Heme Distortions

NP4 complex	pH	ruffling[a]	saddling[a]
Fe^{3+}−H_2O[b]	7.5	−0.55	0.29
Fe^{2+}−H_2O[c]	7.1	−0.37	0.34
Fe^{3+}−NO[b]	5.6	−0.81	0.37
Fe^{2+}−NO[c]	5.6	−0.69	0.36
Fe^{2+}−CO[c]	5.6	−0.62	0.33

[a] Total deviation in angstroms for ruffling (B_{1u}) and saddling (B_{2u}) distortions, using NSD (*24*). [b] Structures from Roberts et al. (*17*). [c] This work.

binds to NP4 (Fe^{3+}) (*10*, *12*, *17*). In addition, as in the case of NO binding to NP4, several water molecules are expelled from the pocket upon CO binding. Overall, the structures of NP4 (Fe^{3+})−NO and NP4 (Fe^{2+})−CO at pH 5.6 are nearly identical, but display a few differences in side-chain positioning. In particular, Leu 130, which swings into the distal pocket upon loop closure (Figure 1B), differs in position by ∼0.5 Å. The Leu 130 side-chain position appears to depend on the distal ligand geometry and adopts slightly different positions in the ferric NO, ferrous NO, CO, and imidazole structures to maintain van der Waals contact with the ligand (this work and refs *12*, *17*). Leu 133, which contacts ligand and heme under all conditions, also shifts slightly in response to the distal ligand position, differing by ∼0.2 Å in the NO and CO complexes.

In both CO structures, the CO ligand has the geometry found in high-resolution structures of carboxymyoglobin (*33*), adopting an essentially linear Fe−C−O bond angle (Figure 3B, Table 3). This is in contrast to the NO geometry found in ferric NP4 complexes, which is bent by ∼20° (*12*, *17*), suggesting the Fe^{2+}−CO bond is stiffer than the Fe^{3+}−NO bond (see Discussion). The heme in the NP4−CO complex, at both low and neutral pH, is distorted from planarity (Figure 4). NSD analyses of the heme conformation reveal that CO binding leads to an increase in the heme ruffling (Table 4), as previously found for NO binding to ferric heme (Table 4, (*17*)). The overall increase in ruffling was similar for both CO binding to ferrous heme and NO binding to ferric heme (∼0.25 Å), but the total ruffling is less for the Fe^{2+}−CO complexes.

Structure of NP4−CO at pH 7.4. The carboxy complex at pH 7.4 was produced in the same manner as for the pH 5.6 complex. However, during refinement, it became clear

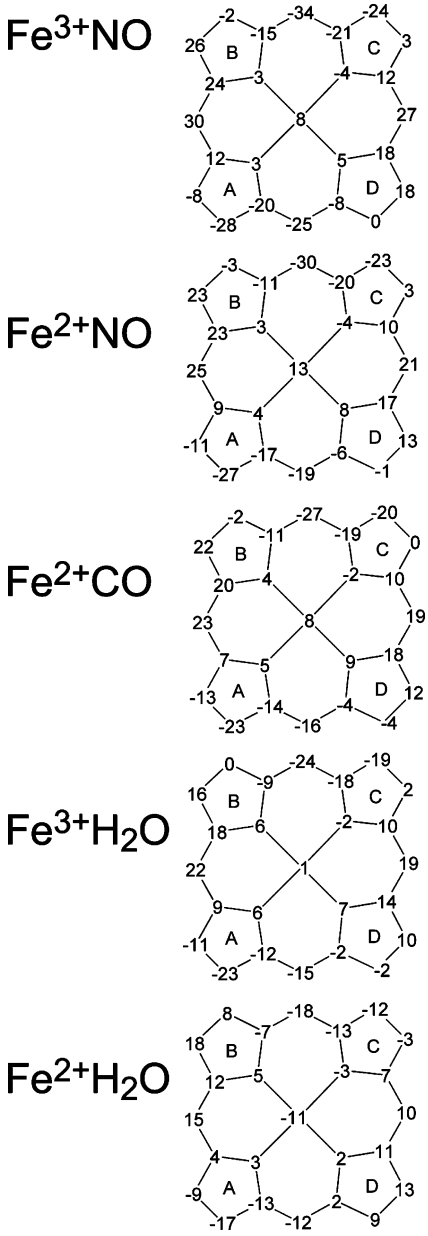

FIGURE 4: Formal core diagrams showing deviations from the mean heme plane, in units of 0.01 Å. Estimated standard errors were calculated for each atom and were generally in the range of 1−2 units (0.01−0.02 Å). Shown (from the top) are the Fe^{3+}−NO, Fe^{2+}−NO, Fe^{2+}−CO, Fe^{3+}−H_2O, and Fe^{2+}−H_2O complexes.

that the CO oxygen was not completely occupied. The reason for this is not clear: incomplete CO saturation or incomplete iron reduction are possible explanations. We refined the structure with occupancies of the CO ligand and of water fixed at 0.75 and 0.25, respectively.

The structure displays a mixture of open and closed conformers, with the open conformation in higher abundance. A similar behavior was observed upon NO binding to NP4 (Fe^{3+}) at the same pH (*12*). The distal pocket of the CO complex at pH 7.4 is filled with one more ordered water molecule compared to the complex at pH 5.6. This water is also present in the aqua ferrous structure, and in previously determined structures when the distal cavity is open, and forms a hydrogen bond with the side chain of Thr 121.

Structure of Ferrous NP4−NO at pH 5.6. Excellent diffraction data were also acquired for the ferrous nitrosyl

complex at pH 5.6 (0.97 Å resolution), obtained by first reducing a ferric NP4 crystal with dithionite and subsequently adding NO (Table 2, Figure 3C). The structure exhibits a closed conformation as observed for the ferric nitrosyl complex (*10*, *12*, *17*).

Bond distances between the metal and the nitrosyl ligand are expected to differ slightly between the two oxidation states, with $Fe^{3+}-NO$ typically ~1.66 Å and $Fe^{2+}-NO$ ~1.72 Å (*34*). The bond length of 1.73 (1) Å found in the present structure (Table 3) is therefore consistent with a ferrous complex. The bond angle of 141 (1)° found in the complex is also consistent with the ferrous complex. Unlike CO, NO coordinates to ferrous iron with a bent geometry. The angle we find in the present complex is typical for an $\{FeNO\}^7$ iron porphyrin system and confirms that a ferrous nitrosyl complex has been formed (*34*−*36*).

Ferrous NO porphyrin complexes usually show a large trans influence, in which the bond distance of the ligand trans to the stronger axial ligand is lengthened by 0.2−0.3 Å as compared to the ferric species, or even becomes dissociated (*34*). A small trans influence is observed in the ferrous nitrosyl complex of NP4, where the proximal bond is lengthened (2.11 (1) Å) compared to that in the ferric derivative (2.013 (9) Å) (*17*), but the bond lengthening is less than that expected for a ferrous NO porphyrin complex. Of the observed lengthening, ~0.05 Å is due to the iron atom moving above the heme plane (Figure 4).

The heme in NP4 (Fe^{2+})−NO is again ruffled, but less so than in the ferric complex (Table 4, Figure 4). Binding of NO to the Fe^{2+} heme induces greater ruffling, compared to the aqua complex, similar to what has been observed for the ferric NP4 complexes.

Occupancy of the Xenon Pocket. Myoglobin contains xenon-accessible cavities that are used by CO for entry and exit to the protein (*37*−*42*). We have identified an analogous cavity in NP4, on the proximal side of the heme; however, it does not appear to play a similar role in ligand entry and escape (*43*). Nonetheless, this cavity is at least partially occupied in three of the four ferrous NP4 structures, the exception being the water-ligated structure where the crystal has not been exposed to either NO or CO. Occupancy of the cavity, as judged by the electron density, decreases in the order: CO complex (pH 5) > CO complex (pH 7) > NO complex (pH 5) ≫ H_2O complex. In previously reported structures, the cavity is either empty or has low occupancy when the crystals have not been treated with NO (*12*, *17*). The cavity is hydrophobic and larger than a CO or NO molecule and approximately spherical, so that no orientational preference exists. Consequently, the electron density appears spherical and difficult to distinguish from a water molecule, and we have therefore modeled it as a water molecule in all structures. Despite this, the increase in electron density on adding NO or CO gas suggests the pocket may be filled with a disordered diatomic molecule.

DISCUSSION

We have characterized the Fe^{2+} heme and its surroundings in the aqua, CO, and NO complexes of NP4 by absorption spectroscopy and ultrahigh-resolution X-ray crystallography. The ferrous complexes exhibit absorption spectra that are similar to the analogous derivatives of myoglobin and exhibit heme coordination geometry that is consistent with a reduced form of the protein. Below, we discuss the effects of iron oxidation state on NP4 heme and protein.

Nonpolar Ligands Induce the Closed Conformer. We previously found that binding of NO, a nonpolar ligand, to ferric NP4 at lower pH leads to a large conformational change that desolvates the ligand binding pocket and protects the nitrosyl adduct from further reaction. This change is independent of heme conformation, since both π-accepting (NO) and π-donating (imidazole) hydrophobic ligands induce the closed conformer (*17*). Here, we show that both NO and CO binding to ferrous NP4 at pH 5.6 induces the same conformational change. The open conformation persists in the ferrous aqua complex despite a change in formal heme charge from +1 to 0 upon reduction (+2 for the iron, −2 for the porphyrin, excluding the propionates). Thus, the detection of ligand polarity for triggering the conformational change appears to be very localized, centered just on the distal pocket and independent of the heme oxidation state. Likewise, the heme reduction potential measurements are also largely insensitive to pH despite the large change in protein conformation that accompanies change in pH, having reduction potentials of −259 mV at pH 5.5 and −278 mV at pH 7.5 for the aqua complexes (*6*).

The structural interpretation is more complicated at neutral pH. We previously showed that NO binding to ferric NP4 at pH 7.4 leads to a mixture of open and closed conformations, with the distal pocket tending toward the closed conformation and the now-charged portions of loops A−B and G−H repelling one another and favoring the open conformation (*12*). Here, we show this behavior also holds for CO binding to ferrous NP4. These data are consistent with a model where loop dynamics are independently governed by pH and ligand polarity.

Kinetic measurements of ligand binding can provide insight into the dynamic behavior of functioning proteins. For ferric rNP, initial NO binding is fast, more so when the distal pocket solvent is more disordered, which occurs in wild-type NP2 (*6*, *8*) and NP4 mutant T121V (*11*), proteins that have more hydrophobic distal pockets. For ferrous NP4, flash-photolysis measurements at pH 8.0 revealed a recombination rate for CO that is similar in magnitude to that for NO binding to ferric NP4 (see Results). Taken together, these data support a model where solvent reorganization is rate-limiting for complex formation rather than bond formation itself, as previously suggested (*6*, *11*). A second phase, previously attributed to loop movements in studies with NO (*6*, *11*), was also detected for CO binding but could not be accurately measured due to the instability of reduced NP4.

All of this is consistent with the physiological role for rNP proteins. The closed conformer, stabilized by nonpolar ligand binding and the low pH of the insect salivary gland (~5), provides protection for the nitrosyl complex, while the open conformer, induced by the neutral pH of the victim, promotes NO release. That loop closure and distal pocket desolvation do indeed protect the nitrosyl adduct is suggested by crystallographic experiments where the ferric NO complex is formed with an open conformer, either due to higher pH (*12*) or mutation (*11*) in NP4, or crystalline contacts in NP1 (*28*) and NP2 (Weichsel, A., and Montfort, W. R., in preparation). In these cases, but not when the closed conformer is completely formed, the nitrosyl heme center is

quite sensitive to photoreduction in the X-ray beam, giving rise to ferrous heme and bent NO geometry.

Heme Pocket Rigidity. The atomic resolution ferrous NP4 structures reported herein allow direct comparison with previously determined ferric structures and the possibility of understanding how the protein influences oxidation state. The geometries of the ferrous heme complexes are, for the most part, the same as found in similar small molecule iron porphyrin complexes (*44*), except that the Fe−His 59 bond length is shorter than expected. In general, the weaker axial ligand in ferrous complexes exhibits a bond lengthening of 0.2−0.3 Å, or even complete dissociation. Iron−histidine bond cleavage, for example, is thought to initiate the conformational change in soluble guanylate cyclase that leads to activation of the protein on NO binding (*45*). In NP4, this lengthening is less pronounced: the Fe−His 59 Nϵ2 distance is 2.11 (1) Å, at least 0.1 Å shorter than expected. We previously suggested that the tightly packed heme pocket in NP4 might interfere with bond lengthening and thereby disfavor reduction of the heme (*17*). The present results are consistent with that possibility, although the energetics associated with this distortion are not yet known. Also noteworthy is that the previously reported ferrous NP4−NO complexes that occurred through photoreduction of the ferric complex in the X-ray beam (*11*, *12*) display the same geometry as the chemically reduced ferrous complex described here.

Fe−NO and −CO Bond Angles. The expected geometry for Fe−XO complexes depends on the total number of metal d and ligand π* electrons (*35*). For example, both Fe^{3+}−NO and Fe^{2+}−CO have $\{FeXO\}^6$ electronic arrangements, which typically display Fe−X−O bond angles of ∼180°, while Fe^{2+}−NO ($\{FeXO\}^7$) complexes typically display bond angles of ∼140°. In ferric NP4−NO (*12*, *17*), the Fe−NO bond is bent ∼20° away from the linear arrangement usually found in small molecule model complexes (*34*). The ferrous CO complexes reported here both display the expected linear bonds (Table 3). The nonpolar side chains in the distal cavity pack around the CO, the ferrous NO, and the ferric NO in a similar fashion, but the position of the side chains contacting the ligands varies. In particular, Leu 130, which is part of the G−H loop and moves into the binding pocket on ligand binding (Figure 1B), shifts in position by 0.5 Å between the ferrous NO and CO structures.

That the Fe^{3+}−NO bond is readily deformed from the linear conformation is clear from quantum mechanical calculations (*46*, *47*) and structures of protein and model Fe^{3+}−NO complexes with bent nitrosyl bonds (*17*, *48*, *49*). For example, the deviation that we see, ∼20°, has been estimated to cost 1−2 kcal mol^{-1} for planar model hemes (*47*). Similarly, distortion of the Fe^{2+}−NO away from the low-energy position requires very little energy (*50*). In contrast, Fe^{2+}−CO is always linear. A search of the Cambridge Structural Database (*44*) reveals all structures of Fe^{2+}−CO porphyrin model complexes to have Fe−C−O angles greater than 172°. Further evidence regarding the differing stiffness of the Fe−CO and Fe−NO bonds in heme proteins is provided by structures of nitric oxide reductase, where the ferrous carboxy complex has an Fe^{2+}−C−O angle of 172° (*51*), while in the ferric nitrosyl complex, the Fe^{3+}−N−O angle is 161° (*48*).

Since a linear arrangement for NP4−CO occurs, a linear arrangement for NO is also sterically possible. That Fe−NO is not linear could simply be due to the softness of the bond and the packing of nearby residues against the NO molecule. However, it is also possible that there is an electronic contribution to bending and, furthermore, that bending serves to protect against reduction of the heme through poorer d−π* orbital overlap between the NO unpaired electron and the metal, as we have previously suggested (*17*). In support of an electronic contribution to bending are recent density functional theory (DFT) modeling studies of five- and six-coordinate ferric NO porphyrin complexes, which show that, as electron-donating substituents are added to the meso heme carbons, the predicted Fe−NO bond angle becomes more bent (*47*, *52*). NO bending is accompanied by a shortening in the two Fe−N (porphyrin) bonds toward which the NO bends by ∼0.01 Å, and a corresponding lengthening in the other two Fe−N (porphyrin) bonds. Crystal structures of model porphyrin complexes with bent Fe−NO conform to this prediction. Unfortunately, despite the high resolution of our protein structures, bond length differences of this magnitude are not discernible, and we cannot confirm (or reject the hypothesis) that a similar effect exists in NP4. That heme distortion alone is not sufficient to induce NO bending seems clear from recent structural and spectroscopic studies of highly distorted model porphyrins, which all display linear Fe^{3+}−NO bonds (*53*).

Although the mechanism by which NO bending in NP4 remains to be uncovered, the effect of bending on reactivity seems more clear. DFT calculations indicate that, as the NO bond is bent, additional electron density builds up on the NO molecule making it less electrophilic and less likely to react with solvent nucleophiles such as water or hydroxyl ion (*47*). Thus, the bent Fe−NO geometry appears to be of functional importance for the storage and transport of the NO molecule.

Heme Distortion and Its Role in Stabilizing the Ferric State. As noted above, the NP4 Fe^{3+} heme is not planar but saddled and ruffled, and the latter distortion, which is predominant, is significantly increased upon the binding of π−acceptor ligands such as CN^- and NO (*17*). The ruffling conformation results from rotation of pyrrole rings about the Fe−N bond and saddling from pyrrole rings tipping out of the heme plan to give a saddle shape. Both ruffling and saddling distortions appear relatively low in energy but correlate with stabilization of the ferric state in both model compounds and proteins (*4*, *13*−*16*). In NP2, mutation of two leucines contacting heme at positions of ruffling distortion (L122V, L132V; equivalent to Leu 123, Leu 133 in NP4, Figure 1B) leads to an ∼50 mV positive shift in reduction potential for the NO complex, consistent with a role for ruffling in the setting of reduction potential (*54*). Nonetheless, despite these promising trends, a direct link between reduction potential and heme distortion in proteins has yet to be described.

In Table 4 and Figure 4, we show overall heme deformations as well as deformations along the heme ruffling and saddling normal modes for both ferrous (this work) and ferric NP4 complexes (*17*). Where direct comparisons are possible, the ferric complexes are more distorted than their ferrous counterparts. The changes are small but significant at this resolution, with all atoms generally lying closer to the least-

squares heme plane in the ferrous structures (Figure 4). The observed change in ruffling is 0.18 Å for the aqua complexes, and 0.12 Å in the NO complexes (Table 4). By way of comparison, the rufflings observed for structures of identical ferric complexes (either NO or aqua), determined independently to differing resolutions using different X-ray wavelengths, agree within ~0.05Å (*11*, *12*, *17*). Interestingly, binding of π−acceptor ligands (NO and CO) to the Fe^{2+} heme led to increased ruffling to the same degree as previously found for π−acceptor ligand binding to the Fe^{3+} heme (*17*), ~0.3 Å, which is 2−3-fold larger than that resulting from the change in oxidation state. The reason for this is not yet known.

The degree of deformation along the ruffling normal mode for the NP4 heme can be summarized in the following order: (Fe^{3+})−NO > (Fe^{2+})−NO ≥ (Fe^{2+})−CO > (Fe^{3+})−H_2O > (Fe^{2+})−H_2O. Thus, the trend we established for NP4 indicates a systematic decrease in ruffling in the reduced state, consistent with the hypothesis that heme distortion favors the ferric state. The mechanism for this may involve the mixing of porphyrin π and iron d orbitals such that the empty d orbital is partially filled, interfering with reduction (recently discussed in detail in ref *4*). The heme remains ruffled in the reduced state, presumably due to protein constraints, which, by this argument, would favor oxidation to Fe^{3+}. Apparently, the factors that lead to increased ruffling on binding π−acceptor ligands NO and CO are still in effect for ferrous heme, since a substantial increase in ruffling occurs relative to the ferrous aqua complex, but to a lesser overall degree than in the ferric state.

Design of an NO Transport Protein. At least three factors appear critical for NO transport by the *Rhodnius* nitrophorins. First, the heme must be stabilized in the ferric state, since binding of NO to ferrous heme is nearly irreversible, particularly in the nitrophorins (K_d = 5−90 fM, (*6*)). The present study suggests that both heme distortion and the restriction of proximal histidine bond lengthening favor the ferric state in the tightly constrained nitrophorin heme pocket. Other factors, such as the placement of negatively charged amino acids near the positively charged ferric heme may also assist in ferric stabilization (*4*). Second, the NO bond is bent, making it less electrophilic and less reactive toward solvent. And third, the distal pocket is desolvated and tightly packed in the NO-bound closed conformation, further discouraging the reductive chemistry of solvent nucleophiles.

ACKNOWLEDGMENT

We thank Jacquie Brailey for protein preparation, Dr. Roger Sperline for assistance in setting up the microspectrophotometer, Drs. John K. Hurley and Gordon Tollin for help with the flash-photolysis experiment. Portions of this research were carried out at the Stanford Synchrotron Radiation Laboratory, a national user facility operated by Stanford University on behalf of the U. S. Department of Energy. Diffraction data were also measured at BioCars Sector 14, Advanced Photon Source, Argonne National Laboratory, which was supported by the U. S. Department of Energy under Contract W-31-109-Eng-38. BioCARS was supported by the National Institutes of Health, National Center for Research Resources, under Grant No. RR07707.

REFERENCES

1. Ribeiro, J. M. C., Hazzard, J. M. H., Nussenzveig, R. H., Champagne, D. E., and Walker, F. A. (1993) Reversible binding of nitric oxide by a salivary heme protein from a bloodsucking insect, *Science 260*, 539−541.
2. Ribeiro, J. M., Andersen, J., Silva-Neto, M. A., Pham, V. M., Garfield, M. K., and Valenzuela, J. G. (2004) Exploring the sialome of the blood-sucking bug *Rhodnius prolixus*, *Insect Biochem. Mol. Biol. 34*, 61−79.
3. Walker, F. A., and Montfort, W. R. (2000) The nitric oxide-releasing heme proteins from the saliva of the blood-sucking insect *Rhodnius prolixus*, in *Advances in Inorganic Chemistry* (Sykes, A. G., and Mauk, G., Eds.) pp 295−358, Academic Press, San Diego, CA.
4. Walker, F. A. (2005) Nitric oxide interaction with insect nitrophorins and thoughts on the electron configuration of the {FeNO}6 complex, *J. Inorg. Biochem. 99*, 216−236.
5. Montfort, W. R., Weichsel, A., and Andersen, J. F. (2000) Nitrophorins and related antihemostatic lipocalins from *Rhodnius prolixus* and other blood-sucking arthropods, *Biochim. Biophys. Acta 1482*, 110−118.
6. Andersen, J. F., Ding, X. D., Balfour, C., Shokhireva, T. K., Champagne, D. E., Walker, F. A., and Montfort, W. R. (2000) Kinetics and equilibria in ligand binding by nitrophorins 1−4: Evidence for stabilization of a NO−ferriheme complex through a ligand-induced conformational trap, *Biochemistry 39*, 10118−10131.
7. Weichsel, A., Andersen, J. F., Champagne, D. E., Walker, F. A., and Montfort, W. R. (1998) Crystal structures of a nitric oxide transport protein from a blood-sucking insect, *Nat. Struct. Biol. 5*, 304−309.
8. Andersen, J. F., and Montfort, W. R. (2000) Crystal structures of nitrophorin 2: A trifunctional antihemostatic protein from the saliva of *Rhodnius prolixus*, *J. Biol. Chem. 275*, 30496−30503.
9. Andersen, J. F., Weichsel, A., Balfour, C. A., Champagne, D. E., and Montfort, W. R. (1998) The crystal structure of nitrophorin 4 at 1.5 Å resolution: Transport of nitric oxide by a lipocalin-based heme protein, *Structure 6*, 1315−1327.
10. Weichsel, A., Andersen, J. F., Roberts, S. A., and Montfort, W. R. (2000) Reversible nitric oxide binding to nitrophorin 4 from *Rhodnius prolixus* involves complete distal pocket burial, *Nat. Struct. Biol. 7*, 551−554.
11. Maes, E. M., Weichsel, A., Andersen, J. F., Shepley, D., and Montfort, W. R. (2004) Role of binding site loops in controlling nitric oxide release: structure and kinetics of mutant forms of nitrophorin 4, *Biochemistry 43*, 6679−6690.
12. Kondrashov, D. A., Roberts, S. A., Weichsel, A., and Montfort, W. R. (2004) Protein functional cycle viewed at atomic resolution: Conformational change and mobility in nitrophorin 4 as a function of pH and NO binding, *Biochemistry 43*, 13637−13647.
13. Shelnutt, J. A., Song, X.-Z., Ma, J.-G., Jia, S.-L., Jentzen, W., and Medforth, C. J. (1998) Nonplanar porphyrins and their significance in proteins, *Chem. Soc. Rev. 27*, 31−41.
14. Kadish, K. M., Van Camelbecke, E., and Royal, G. (2000) Electrochemistry of metalloporphyrins in nonaqueous media, in *The Porphyrin Handbook* (Kadish, K. M., Smith, K. M., and Guilard, R., Eds.) pp 3−125, Academic Press, San Diego, CA.
15. Safo, M. K., Nesset, M. J. M., Walker, F. A., Debrunner, P. G., and Scheidt, W. R. (1997) Models of the cytochromes. Axial ligand orientation and complex stability in iron(II) porphyrinates: The case of the noninteracting d(pi) orbitals, *J. Am. Chem. Soc. 119*, 9438−9448.
16. Nesset, M. J. M., Shokhirev, N. V., Enemark, P. D., Jacobson, S. E., and Walker, F. A. (1996) Models of the cytochromes. Redox properties and thermodynamic stabilities of complexes of "hindered" iron(III) and iron(II) tetraphenylporphyrinates with substituted pyridines and imidazoles, *Inorg. Chem. 35*, 5188−5200.
17. Roberts, S. A., Weichsel, A., Qiu, Y., Shelnutt, J. A., Walker, F. A., and Montfort, W. R. (2001) Ligand-induced heme ruffling and bent NO geometry in ultra-high-resolution structures of nitrophorin 4, *Biochemistry 40*, 11327−11337.
18. Andersen, J. F., Champagne, D. E., Weichsel, A., Ribeiro, J. M. C., Balfour, C. A., Dress, V., and Montfort, W. R. (1997) Nitric oxide binding and crystallization of recombinant nitrophorin I, a nitric oxide transport protein from the blood-sucking bug *Rhodnius prolixus*, *Biochemistry 36*, 4423−4428.

19. Antonini, E., and Brunori, M. (1971) *Hemoglobin and Myoglobin in Their Reactions with Ligands*, Vol. 21, North-Holland Publ. Co., Amsterdam, The Netherlands.
20. Pflugrath, J. W. (1999) The finer things in X-ray diffraction data collection, *Acta Crystallogr., Sect. D 55*, 1718−1725.
21. Collaborative Computational Project Number 4 (1994) The CCP4 suite: Programs for protein crystallography, *Acta Crystallogr., Sect. D 50*, 760−763.
22. Sheldrick, G. M., and Schneider, T. R. (1997) SHELXL: High −resolution refinement, *Methods Enzymol. 277*, 319−343.
23. Jones, T. A., Zou, J. Y., Cowan, S. W., and Kjelgard, M. (1991) Improved methods for building protein models in electron density maps and the location of errors in these models, *Acta Crystallogr., Sect. A 47*, 110−119.
24. Jentzen, W., Song, X.-Z., and Shelnutt, J. A. (1997) Structural characterization of synthetic and protein-bound porphyrins in terms of the lowest-frequency normal coordinates of the macrocycle, *J. Phys. Chem. B. 101*, 1684−1699.
25. Kraulis, P. J. (1991) MOLSCRIPT: A program to produce both detailed and schematic plots of protein structures, *J. Appl. Crystallogr. 24*, 946−950.
26. Esnouf, R. M. (1997) An extensively modified version of MolScript that includes greatly enhanced coloring capabilities, *J. Mol. Graphics Modell. 15*, 132−134, 112−113.
27. Merritt, E. A., and Murphy, M. E. P. (1994) Raster3D version 2.0—a program for photorealistic molecular graphics, *Acta Crystallogr., Sect. D 50*, 869−873.
28. Ding, X. D., Weichsel, A., Andersen, J. F., Shokhireva, T. K., Balfour, C., Pierik, A. J., Averill, B. A., Montfort, W. R., and Walker, F. A. (1999) Nitric oxide binding to the ferri- and ferroheme states of nitrophorin 1, a reversible NO-binding heme protein from the saliva of the blood-sucking insect, *Rhodnius prolixus*, *J. Am. Chem. Soc. 121*, 128−138.
29. Addison, A. W., and Stephanos, J. J. (1986) Nitrosyliron(III) hemoglobin: Autoreduction and spectroscopy, *Biochemistry 25*, 4104−4113.
30. Romberg, R. W., and Kassner, R. J. (1979) Nitric oxide and carbon monoxide equilibria of horse myoglobin and (*N*-methylimidazole)-protoheme. Evidence for steric interaction with the distal residues, *Biochemistry 18*, 5387−5392.
31. Kaneko, Y., Yuda, M., Iio, T., Murase, T., and Chinzei, Y. (1999) Kinetic analysis on nitric oxide binding of recombinant Prolixin-S, a nitric oxide transport protein from the bloodsucking bug, *Rhodnius prolixus*, *Biochim. Biophys. Acta 1431*, 492−499.
32. Springer, B. A., Sligar, S. G., Olson, J. S., and Phillips, G. N. (1994) Mechanisms of Ligand Recognition in Myoglobin, *Chem. Rev. 94*, 699−714.
33. Vojtechovsky, J., Chu, K., Berendzen, J., Sweet, R. M., and Schlichting, I. (1999) Crystal structures of myoglobin-ligand complexes at near-atomic resolution, *Biophys. J. 77*, 2153−2174.
34. Scheidt, W. R., and Ellison, M. K. (1999) The synthetic and structural chemistry of heme derivatives with nitric oxide ligands, *Acc. Chem. Res. 32*, 350−359.
35. Enemark, J. H., and Feltham, R. D. (1974) Principles of structure, bonding, and reactivity for metal nitrosyl complexes, *Coord. Chem. Rev. 13*, 339−406.
36. Spiro, T. G., Zgierski, M. Z., and Kozlowski, P. M. (2001) Stereoelectronic factors in CO, NO and O2 binding to heme from vibrational spectroscopy and DFT analysis, *Coord. Chem. Rev. 219−221*, 923−936.
37. Tilton, R. F., Jr., Kuntz, I. D., Jr., and Petsko, G. A. (1984) Cavities in proteins: Structure of a metmyoglobin−xenon complex solved to 1.9 Å, *Biochemistry 23*, 2849−2857.
38. Nienhaus, K., Deng, P., Kriegl, J. M., and Nienhaus, G. U. (2003) Structural dynamics of myoglobin: Spectroscopic and structural characterization of ligand docking sites in myoglobin mutant L29W, *Biochemistry 42*, 9633−9646.
39. Ostermann, A., Waschipky, R., Parak, F. G., and Nienhaus, G. U. (2000) Ligand binding and conformational motions in myoglobin, *Nature 404*, 205−208.
40. Schotte, F., Lim, M., Jackson, T. A., Smirnov, A. V., Soman, J., Olson, J. S., Phillips, G. N., Jr., Wulff, M., and Anfinrud, P. A. (2003) Watching a protein as it functions with 150-ps time-resolved x-ray crystallography, *Science 300*, 1944−1947.
41. Bourgeois, D., Vallone, B., Schotte, F., Arcovito, A., Miele, A. E., Sciara, G., Wulff, M., Anfinrud, P., and Brunori, M. (2003) Complex landscape of protein structural dynamics unveiled by nanosecond Laue crystallography, *Proc. Natl. Acad. Sci. U.S.A. 100*, 8704−8709.
42. Brunori, M., Bourgeois, D., and Vallone, B. (2004) The structural dynamics of myoglobin, *J. Struct. Biol. 147*, 223−234.
43. Nienhaus, K., Maes, E. M., Weichsel, A., Montfort, W. R., and Nienhaus, G. U. (2004) Structural dynamics controls nitric oxide affinity in nitrophorin 4, *J. Biol. Chem. 279*, 39401−39407.
44. Allen, F. H. (2002) The cambridge structural database: A quarter of a million crystal structures and rising, *Acta Crystallogr., Sect. B 58*, 380−388.
45. Denninger, J. W., and Marletta, M. A. (1999) Guanylate cyclase and the •NO/cGMP signaling pathway, *Biochim. Biophys. Acta 1411*, 334−350.
46. Scherlis, D. A., Cymeryng, C. B., and Estrin, D. A. (2000) Nitric oxide binding to ferric cytochrome P450: A computational study, *Inorg. Chem. 39*, 2352−2359.
47. Linder, D. P., and Rodgers, K. R. (2005) Fe−N−O structure and bonding in six-coordinate $\{FeNO\}^6$ porphyrinates containing imidazole: Implications for reactivity of coordinated NO, *Inorg. Chem. 44*, 1367−1380.
48. Shimizu, H., Obayashi, E., Gomi, Y., Arakawa, H., Parks, S.-Y., Nakamura, H., Adachi, S.-i., Shoun, H., and Shiro, Y. (2000) Proton delivery in NO reduction by fungal nitric-oxide reductase, *J. Biol. Chem. 275*, 4816−4826.
49. Richter-Addo, G. B., Wheeler, R. A., Hixson, C. A., Chen, L., Khan, M. A., Ellison, M. K., Schulz, C. E., and Scheidt, W. R. (2001) Unexpected nitrosyl-group bending in six-coordinate [M(NO)](6) sigma-bonded aryl(iron) and -(ruthenium) porphyrins, *J. Am. Chem. Soc. 123*, 6314−6326.
50. Coyle, C. M., Vogel, K. M., Rush, T. S., Kozlowski, P. M., Williams, R., Spiro, T. G., Dou, Y., Ikeda-Saito, M., Olson, J. S., and Zgierski, M. Z. (2003) FeNO structure in distal pocket mutants of myoglobin based on resonance Raman spectroscopy, *Biochemistry 42*, 4896−4903.
51. Shimizu, H., Park, S. Y., Shiro, Y., and Adachi, S. (2002) X-ray structure of nitric oxide reductase (cytochrome P450nor) at atomic resolution, *Acta Crystallogr., Sect. D 58*, 81−89.
52. Linder, D. P., Rodgers, K. R., Banister, J., Wyllie, G. R., Ellison, M. K., and Scheidt, W. R. (2004) Five-coordinate Fe(III)NO and Fe(II)CO porphyrinates: Where are the electrons and why does it matter? *J. Am. Chem. Soc. 126*, 14136−14148.
53. Ellison, M. K., Schulz, C. E., and Scheidt, W. R. (2002) Nitrosyliron(III) porphyrinates: Porphyrin core conformation and FeNO geometry. Any correlation? *J. Am. Chem. Soc. 124*, 13833−13841.
54. Shokhireva, T., Berry, R. E., Uno, E., Balfour, C. A., Zhang, H., and Walker, F. A. (2003) Electrochemical and NMR spectroscopic studies of distal pocket mutants of nitrophorin 2: Stability, structure, and dynamics of axial ligand complexes, *Proc. Natl. Acad. Sci. U.S.A. 100*, 3778−3783.

BI0506573